Mechanisms of Ageing and Development 217 (2024) 111897

Contents lists available at ScienceDirect

Mechanisms of Ageing and Development

journal homepage: www.elsevier.com/locate/mechagedev

The cGAS-STING signaling pathway is modulated by urolithin A

H.B. Madsen [a], J-H. Park [b], X. Chu [b], Y. Hou [b,d], Z. Li [a], L.J. Rasmussen [a], D.L. Croteau [b,c], V.A. Bohr [a,b,*], M. Akbari [a,e,**]

[a] Center for Healthy Aging, Department of Cellular and Molecular Medicine, SUND, University of Copenhagen, 2200, Copenhagen N, Denmark
[b] Section on DNA repair, National Institute on Aging, 251 Bayview Blvd, Baltimore, MD, USA
[c] Laboratory of Genetics and Genomics, Computational Biology and Genomics Core, National Institute on Aging, 251 Bayview Blvd, Baltimore, USA
[d] Institute for Regenerative Medicine, Shanghai East Hospital, Shanghai Key Laboratory of Signaling and Disease Research, Frontier Science Center for Stem Cell Research, School of Life Sciences and Technology, Tongji University, Shanghai 200092, China
[e] Department of Medical Biology, Faculty of Health Sciences, UiT-The Arctic University of Norway, Tromsø, Norway

ARTICLE INFO

Keywords:
CGAS-STING
Urolithin A
Inflammation
Autophagy
Endoplasmic reticulum

ABSTRACT

During aging, general cellular processes, including autophagic clearance and immunological responses become compromised; therefore, identifying compounds that target these cellular processes is an important approach to improve our health span. The innate immune cGAS-STING pathway has emerged as an important signaling system in the organismal defense against viral and bacterial infections, inflammatory responses to cellular damage, regulation of autophagy, and tumor immunosurveillance. These key functions of the cGAS-STING pathway make it an attractive target for pharmacological intervention in disease treatments and in controlling inflammation and immunity. Here, we show that urolithin A (UA), an ellagic acid metabolite, exerts a profound effect on the expression of STING and enhances cGAS-STING activation and cytosolic DNA clearance in human cell lines. Animal laboratory models and limited human trials have reported no obvious adverse effects of UA administration. Thus, the use of UA alone or in combination with other pharmacological compounds may present a potential therapeutic approach in the treatment of human diseases that involves aberrant activation of the cGAS-STING pathway or accumulation of cytosolic DNA and this warrants further investigation in relevant transgenic animal models.

1. Introduction

With aging, cellular processes such as DNA damage responses, oxidative stress pathways, cellular degradation and immune signaling become compromised (Bartleson et al., 2021). Targeting these pathways for therapeutical intervention is important to improve our health span.

An increase in persistent low-grade, systemic inflammation is observed with age, which is thought to compromise our ability to fight infections and contribute to the development of other age-related diseases (Bartleson et al., 2021). The innate immune system has evolved different types of sensors to detect nucleic acids of invading pathogens to activate a defense response in the infected cell (Zahid et al., 2020). The cytosolic DNA-sensing receptor cyclic GMP-AMP Synthase (cGAS) and its effector protein, Stimulator of Interferon Genes (STING), become activated by cytosolic double-stranded DNA in various immune and non-immune cell types (Gao et al., 2013; Sun et al., 2013; Wu et al., 2013). The binding of cGAS to free DNA activates the production of 2´,3´ cyclic GAMP (cGAMP), a second messenger, that binds to and activates STING, resulting in the transport of STING from the endoplasmic reticulum (ER) to the trans-Golgi network, where it activates TANK-binding kinase 1 (TBK1). Activated TBK1 phosphorylates the transcription factor Interferon regulatory factor 3 (IRF3) leading to the dimerization and nuclear localization of IRF3 (Ishikawa and Barber, 2008). TBK1 and its homolog IκB kinase epsilon can activate the IKK complex, which releases NF-κB from its cytoplasmic inhibitor IκB, to translocate to the nucleus, where IRF3 and NF-κB synergize to activate the expression of type I

Abbreviations: cGAMP, 2´,3´cyclic GAMP; cGAS, cyclic GMP-AMP Synthase; ER, Endoplasmic Reticulum; IRF3, Interferon regulatory factor 3; ISGs, interferon stimulated genes; STAT1, Signal transducer and activator of transcription 1; STING, Stimulator of Interferon Genes; TBK1, TANK-binding kinase 1; IFNI, type I interferon; UA, Urolithin A; WB, Western blot.

* Correspondence to: DNA Repair Section, National Institute on Aging, NIH, 251 Bayview Blvd, Suite 100, Rm 06B133, Baltimore, MD 21224, USA.
** Correspondence to: Department of Medical Biology, Faculty of Health Sciences, UiT-The Arctic University of Norway, NO 9037 Tromsø, Norway.
E-mail addresses: vbohr@sund.ku.dk (V.A. Bohr), mansour.akbari@uit.no (M. Akbari).

https://doi.org/10.1016/j.mad.2023.111897
Received 30 June 2023; Received in revised form 21 November 2023; Accepted 13 December 2023
Available online 16 December 2023

interferon (IFNI) and inflammatory genes. IFNI subsequently activates the expression of interferon-stimulated genes (ISGs), such as Signal transducer and activator of transcription 1 (STAT1), via endocrine and paracrine activation of specific IFNI membrane receptors on the infected and uninfected adjacent cells, respectively, collectively promoting innate and adaptive defense responses to infection (Ishikawa and Barber, 2008; Hopfner and Hornung, 2020).

Autophagy is an evolutionarily conserved process for degrading damaged organelles, protein aggregates, and more (Galluzzi et al., 2017). In autophagy, cytosolic components are engulfed into double-membrane autophagosome vesicles, which are subsequently delivered to lysosomes for degradation (Galluzzi et al., 2017).

Recent studies have shown that the IFN signaling function of STING is important, and that the promotion of cellular autophagy in response to cytosolic viral dsDNA constitutes the evolutionarily conserved primordial function of STING (Gui et al., 2019; Liu et al., 2019). Moreover, autophagic degradation of STING following TBK1 activation controls the IFNI response and acts as negative feedback to prevent sustained innate immune signaling (Konno et al., 2013; Liu et al., 2019). Thus, a dynamic interplay between autophagy and STING has evolved to control the autophagic flux and innate immunity.

It has long been known that inflammation constitutes a critical component of tumor progression and that various immune cells infiltrate malignant tumors (Demaria et al., 2019). Genome instability is a hallmark of cancer development and is often associated with the release of various forms of nuclear DNA into the cytoplasm (Hatch et al., 2013; Li et al., 2021a). The aberrant presence of DNA in the cytoplasm and activation of cGAS-STING signaling is thought to be a critical anticancer immune response (Amouzegar et al., 2021). Thus, impaired cGAS-STING signaling in various cancer types, including colon and gastric cancers, have been reported (Xia et al., 2016; Song et al., 2017). However, in most tumors, the downstream IFNI signaling rather than the expression of cGAS and STING proteins appears to be impaired (Vashi and Bakhoum, 2021). The relationship between cGAS-STING activity, tumor development, and metastasis is complex and likely highly context dependent (Bakhoum et al., 2018; Hong et al., 2022).

As the central function of STING in key cellular processes and in various diseases is increasingly investigated, the identification and development of compounds to control cGAS-STING have attracted much attention recently (Liu et al., 2020).

Urolithin A (UA) is a gut microbial metabolite produced from ellagic acid, a polyphenol found in food, fruits, and nuts (Cerdá et al., 2005). UA has been reported to display modulatory properties on several processes affected by age, including oxidative stress, cell proliferation, inflammation, and autophagy (Komatsu et al., 2018; Norden and Heiss, 2019; Toney et al., 2021). Here we show that UA exerts significant modulatory effects on the cGAS-STING pathway and autophagy in human cell lines, likely through stimulation of STING expression.

2. Material and methods

Synthetic oligonucleotides were from TAG Copenhagen. Human microglia cell line HMC3, and UA were obtained from Merck. 2´3´-cGAMP was from InvivoGen.

2.1. Cell culture and treatments

HMC3 cells (ATCC CRL-3304) were cultured in Minimum Essential Medium Eagle (Merck) containing 10% fetal bovine serum and 1% GlutaMAX (Thermo Fisher Scientific). MLH1 deficient HCT116 cells were cultured in McCoy's 5 A Modified Medium, containing 1% GlutaMAX and 10% FBS.

We used double-strand linear DNA and cGAMP to stimulate the cGAS-STING pathway. pAcGFP1-Hyg-N1 vector (Clontech) was digested with *Eco*RI and *Ase*I. The digested plasmids were mixed and purified using NucleoSpin Plasmid Mini Kit (Macherey Nagel). This results in a mixture of DNA fragments of 236, 1143, 1604, 2209, 2811, and 3639 bp that were used to stimulate cGAS-STING by transfection, "DNA".

Cells (1.5×10^6) were seeded on 10-cm dishes. Next day, the cells were transfected with 500 ng digested DNA using Lipofetcamine 3000 (Thermo Fisher Scientific). Cells were harvested by trypsin treatment 12 h post-transfection. One third of the cells were used to purify RNA (RNeasy mini kit, Qiagen) where indicated, and the rest were used to prepare whole cell extracts (WCE).

For cGAMP-mediated STING stimulation, cells were cultured in full medium containing 30 μM cGAMP for 8 h.

For UA treatment, cells were kept in growth medium containing 10 μM UA for five days, for cells to adapt to gene expression changes, and then in medium with 12.5 μM UA for 48 h prior to cGAS-STING stimulation by dsDNA (500 ng) or cGAMP (30 μM).

2.2. NanoString gene expression analysis

For gene expression analysis, we used the human neuroinflammation panel (XT-CSO-MNROI1–12), which contains transcripts of 770 neuroinflammatory genes. NanoString analysis was performed on the human microglial HMC3 cells with vehicle, DNA, or UA treatment. Total RNA was purified from cells using RNeasy Mini Kit (Qiagen) as per the manufacturer's protocol. Purified RNA was quantified on a NanoDrop ND-1000 spectrophotometer and diluted in nuclease-free water to 20 ng/uL. It was hybridized in CodeSet mix carrying hybridization buffer, Reporter Code Set, and Capture Probe Set at 65 °C for 16 to 24 h in a thermal cycler. Hybridized RNA was quantified on a NanoString nCounter Prep Station and Digital Analyzer Max System with the manufacturer's high sensitivity protocol. Hybridized RNA samples were loaded onto the nCounter Prep Station for immobilization in the sample cartridge (NanoString Technologies, MAN-C0035–07). The prep station can process up to 12 samples run in approximately 2.5 to 3 h, depending on which protocol was used. Next, the nCounter Digital Analyzer, which is a multi-channel epifluorescence scanner, collected data by taking images of the immobilized fluorescent reporters in the sample cartridge with a CCD camera through a microscope objective lens. The results were downloaded from the nCounter Digital Analyzer in RCC file format.

Meta analysis of the NanoString human neuroinflammation panel was analyzed by ROSALIND® (https://rosalind.bio/), with a HyperScale architecture developed by ROSALIND, Inc. (San Diego, CA). Read distribution percentages, violin plots, identity heatmaps, and sample MDS plots were generated as part of the QC step. Normalization, fold changes and p-values were calculated using criteria provided by Nanostring. ROSALIND® follows the nCounter® Advanced Analysis protocol of dividing counts within a lane by the geometric mean of the normalizer probes from the same lane. Housekeeping probes to be used for normalization are selected based on the geNorm algorithm as implemented in the NormqPCR R. Fold changes and p-values were calculated using the fast method as described in the nCounter® Advanced Analysis 2.0 User Manual. Data was analyzed by fold difference. A fold-change cut-off of 1.5 was used and an adj. p-value ≤ 0.05 was considered statistically significant. GEO access number is GSE224258.

2.3. Quantitative PCR (qPCR) analysis of gene expression

Total RNA was purified using RNeasy Mini Kit (Qiagen). Complementary DNA was prepared using Maxima Reverse Transcriptase and Oligo dT (12−18) (Thermo Fisher Scientific- Life tech). qPCR was performed using a real-time PCR kit (Bio-Rad1725271) following the manufacturer's protocol. The nucleotide sequence of the primers is indicated in Supplementary Table 1.

2.4. Immunofluorescence

HMC3 cells were grown on Poly-L-lysine (P1399, Merck) coated

eight-chambered object glass (177402, Thermo Scientific) overnight. Cells were transfected with DNA as described above for 12 h, washed in PBS and fixed for 10 min in 4% paraformaldehyde (sc-281692, Santa Cruz) at room temperature. Cells were blocked in 2% BSA (0332, VWR) dissolved in PBS then permeabilized in 0.1% Triton X-100 (T8787, sigma) in PBS. Primary antibodies: IRF3 (sc-33641, Santa Cruz), pSTING (50907 S, Cell Signaling), TGN46 (MA3–063, Thermo Fisher) and Calreticulin (PA5–25922, Invitrogen) were diluted in PBS containing 1% BSA and incubated with cells over night at 4 °C followed by washing in PBS. Secondary Alexa488- and Alexa568-conjugated goat-anti-mouse (A11029, Invitrogen) and goat-anti-rabbit (A11011, Invitrogen) antibodies and DAPI (D9542, Merck) were incubated with cells for 1–2 h at room temperature. The chamber was removed, and cells were mounted (S3023, Dako). Slides were imaged with an upright Leica DM4B microscope with a Leica EL6000 external light source and a Leica DFC365 camera. Images were analyzed using an ImageJ (Version v 1.53 m) macro. Briefly, the macro uses the DAPI channel to select the nuclear regions and measures the intensity of the IRF3 signals. The percentage of nuclei positive for IRF3 staining above a certain threshold was calculated using Microsoft Excel software. The pSTING, TGN46, and Calreticulin signals were measured and normalized to the number of cells. GraphPad Prism V9.2 was used for plotting and statistical analysis.

2.5. TAMRA-tagged DNA degradation assay

We prepared TAMRA-tagged PCR-based DNA substrates for microscopy analysis. The substrates contained TAMRA either at 5´(Substrate I), or at 3´(Substrate II), or at both ends (Substrate III). Each PCR mix (50 µl) contained; 10 pmol of each primer (Supplementary Table 2), 200 µM of each dNTP, 2.5 mM $MgCl_2$, 1 U Dream Taq PCR polymerase (Thermo Fisher Scientific), and 100 ng DNA template (pGEM-3Zf+, Promega). Amplicon 1.967 kb. PCR profile; 94° C 1 min, then 35 cycles of 94° C 30 s, 55° C 30 s, 72° C 1.5 min, and a final step72 °C for 3 min. The PCR products were purified using QIAamp DNA Mini Kit (QIAGEN). HMC3 cells were treated with UA as described above. Before addition of TAMRA-tagged DNA, medium was changed to HBSS with calcium and magnesium, without Phenol Red (Cytiva) supplemented with 20 mM HEPES (Sigma) and imaged every 90 min using the Incucyte® Zoom live cell analysis system. A basic analysis using the Incucyte® Zoom software was conducted to score the total red object integrated intensity (RCU x μm^2/image) over time.

2.6. Western blot

Whole cell extracts were prepared by suspending cell pellets in 20 mM HEPES-KOH, pH 7.5, 150 mM KCl, 10% glycerol, 1% Triton X-100, 1% IGEPAL, 1 mM EDTA, 1 mM DTT, EDTA-free Complete protease inhibitor cocktail (Merck), and PhosSTOP (Merck) and left on ice for 60 min. Cell debris was pelleted at 15,000 g for 15 min, and the supernatant (WCE) was collected.

The extracts were separated in Tris-glycine SDS gels and transferred onto PVDF membrane. The primary antibodies used were STING (13647 S), phospho-STING (Ser366, 19781 S), TBK1 (3504 S), phospho-TBK1 (Ser172, 5483 S), phospho-IRF-3 (Ser386, 37829 S), Stat1 (9172 S), phospho-Stat1 (Tyr701, 9167 S), SQSTM1/p62 (5114 S), Ulk1 (6439 S), phospho-ULK1 (Ser555, 5869), NF-κB p65 (L8F6, 6956 S) were from Cell Signaling. ATG9A (ab108338) was from Abcam. IRF3 (SL-12, sc-33641) was from Santa Cruz, LC3 (NB600–1384) was from Novus Biologicals, and ACTIN (A5441) was from Merck. Uncropped images of the gels are provided in Supplementary Figure 6.

2.7. Statistical analysis

Error bars represent standard error (SE) as indicated in the figure legends. Data were processed, and statistical analyses were performed in Excel or GraphPad Prism. Statistical analysis of differences between two groups was performed using a two-tailed, unpaired t-test. For comparison between multiple groups, two-way ANOVA analysis was applied. Significance is scored as ns $p > 0.05$, * $p < 0.05$, * * $p < 0.01$, * ** $p < 0.001$. The number of biological replicates, n, is indicated in each figure legend.

3. Results

HMC3 cells are SV40-immortalized human embryonic microglia cells, and microglia are the resident immune cells in the brain. HMC3 cells express the key inflammatory proteins of the cGAS-STING pathway and show a robust response to cytosolic double-strand linear DNA (Fig. 1). HMC3 cells are widely used as a model for human microglia cells in neurobiological studies. Thus, these cells were used to evaluate the microglial response to UA. UA treatment did not change viability or nuclear size, as shown in Supplementary Figure 1.

3.1. UA stimulates the expression of STING and enhances cGAS-STING signaling

UA is a polyphenol and an ellagic acid metabolite (Cerdá et al., 2005). It modulates various processes, including inflammation and autophagy (Toney et al., 2021; Qiu et al., 2022); however, a modulatory effect of UA on cGAS-STING signaling has not been reported previously.

UA treatment significantly increased the level of STING protein, while the level of key downstream proteins TBK1, IRF3, and STAT1 was not significantly affected by this treatment compared to control (UTR) (Fig. 1A and Supplementary Figure 2). The level of STING was reduced in DNA-stimulated cells probably because of the degradation of STING by a negative feedback control mechanism (Zhong et al., 2009; Wang et al., 2015). UA treatment maintained the level of STING in DNA-stimulated cells comparable to the level of DNA-treated control cells (Fig. 1A and B). DNA treatment stimulated STING activation by phosphorylation, which was significantly enhanced by UA treatment in relation to ACTIN (Fig. 1A and C), but not in relation to total STING, probably due to increased expression of STING (Fig. 1A and D). Phosphorylation of IRF3 protein downstream of STING activation was also increased in combined DNA- and UA-treatment (Fig. 1E), however, TBK1 and STAT1 were not significantly affected (Supplementary Figure 2). Phosphorylation of NF-κB downstream of STING activation in response to DNA stimulation was significantly decreased by UA treatment (Fig. 1A, F and G).

Next, we carried out immunofluorescence and image analysis of pSTING and IRF3 in response to UA treatment and DNA stimulation (Fig. 1H-J). In line with the WB results, both the level of pSTING and nuclear IRF3 were significantly elevated in the combined UA-treated and DNA-stimulated cells compared with only DNA-stimulated cells. Furthermore, UA alone enhanced pSTING intensity compared to untreated control cells (Fig. 1I), without resulting in significantly elevated levels of nuclear IRF3 (Fig. 1J).

To determine whether the observed effect of UA on the STING level was through altered degradation and turnover rate of STING, or if it involved elevated gene transcription and mRNA levels, we carried out qPCR analysis of STING gene (*TMEM173*) expression, for simplicity referred to as *STING*. The results showed that UA treatment significantly enhanced *STING* expression (Fig. 2A). Moreover, by maintaining the STING levels following DNA stimulation (Fig. 1B), UA treatment significantly enhanced the expression of *IFNβ* and *CXCL10* genes (Fig. 2B-C), downstream of IRF3 activation (Sun et al., 2009) and STAT1 (Burke et al., 2013).

This data is in line with the WB- and immunofluorescence results, showing no detectable effect of UA treatment alone on the activation of IRF3 (Fig. 1E and J, UTR group).

In an ongoing project, we are investigating the effect of UA on the pathology of Alzheimer's disease, a neurodegenerative disease associated with neuroinflammation (Laurent et al., 2018), using an APP/PS1

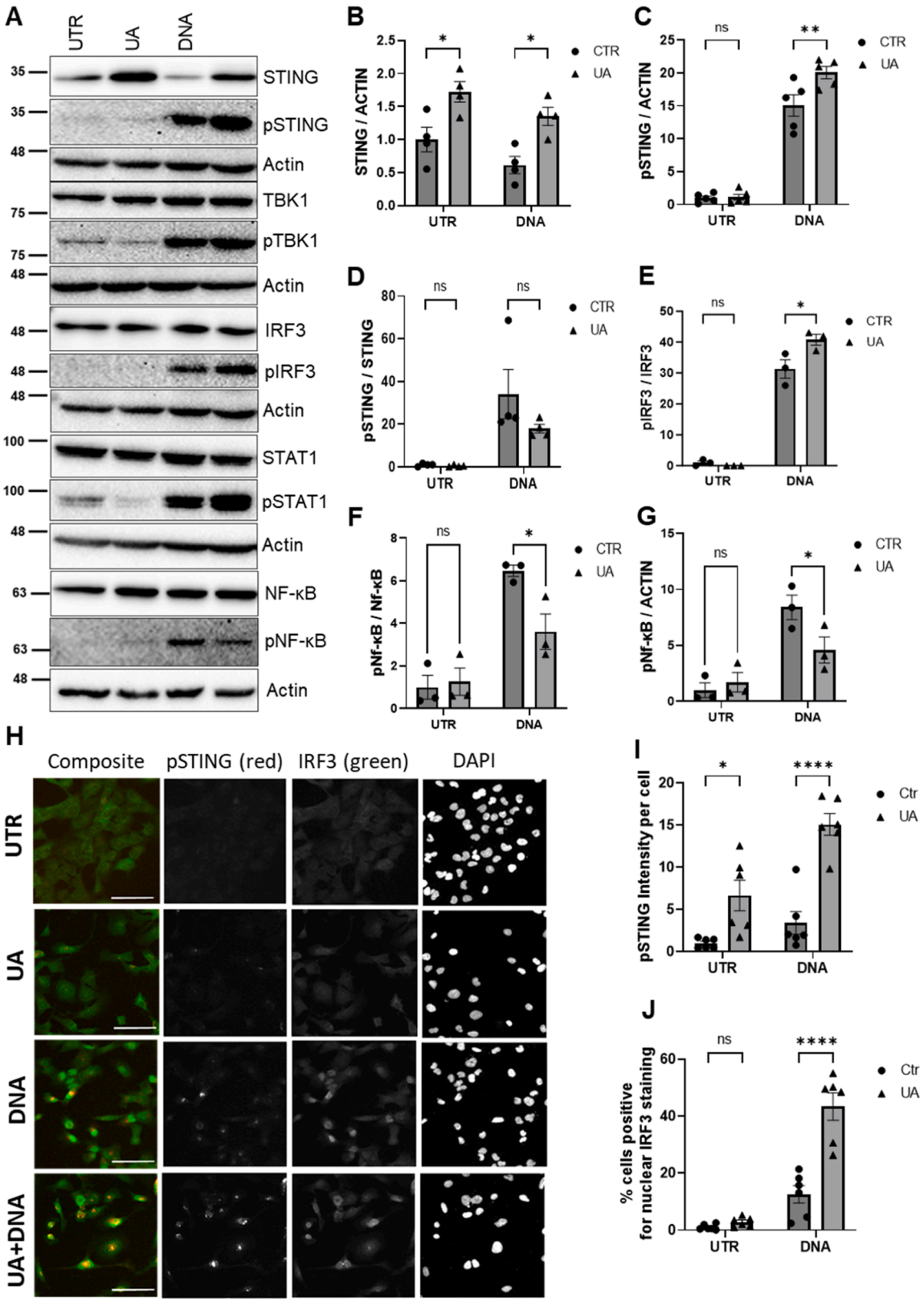

Fig. 1. UA stimulates the expression but not the activation of STING and enhances cGAS-STING signaling. (A) WB showing effect of UA treatment and combined UA treatment and DNA transfection on key cGAS-STING pathway factors in HMC3 microglia cells compared to control (UTR). (B-G) Protein levels of total and phosphorylated forms of STING (n = 4), IRF3 (n = 3) and NF-κB (n = 3) were quantified and normalized. (H) Representative images of HMC3 cells stimulated with UA and/or DNA and stained for pSTING (red), IRF3 (green) and DAPI. Image analysis was used to score the pSTING intensity. Scalebar = 50 μm. (I) and the percentage of IRF3-positive nuclei (J) scored by an imageJ algorithm (n = 6) with two-way ANOVA statistical analysis.

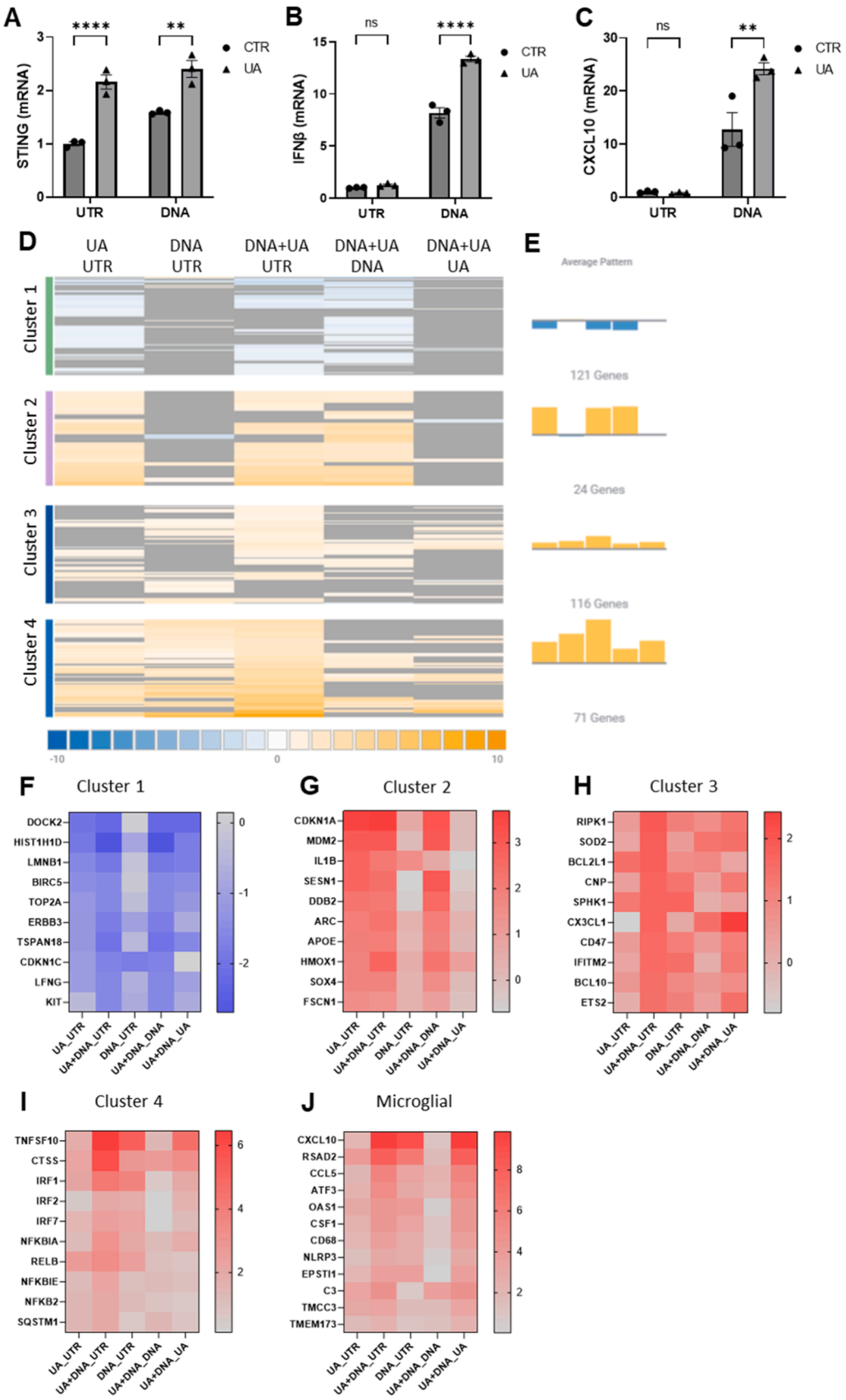

(caption on next page)

Fig. 2. Gene expression analysis shows that UA upregulates several microglial- and neuroinflammation related genes. HCM3 cells were treated with UA or UA- and DNA combined before RNA was harvested. qPCR analysis was conducted for STING (A), IFNβ (B) and CXCL10 (C) expression relative to control (UTR) (n = 3). Graphs were analyzed using two-way ANOVA. (D) Furthermore, Rosalind meta-analysis of gene expression patterns from the NanoString neuroinflammation panel identifies four clusters (n = 3). (E) Summary of the average gene expression for the cluster across the whole dataset. (F – I) Top changed genes from each cluster identified in (D). (J) Top changed microglial genes.

double transgenic mouse model of human Alzheimer disease (specifically expressing human amyloid precursor protein and human mutant presenilin1 in neurons). We treated the mice with UA for five months before RNA was purified from the liver and used in qPCR expression analysis of *STING*, *IFNβ* and *CXCL10* genes. *STING* expression tended to be elevated while *IFNβ* and *CXCl10* levels tended to decline (Supplementary Figure 3). These results are somewhat similar to the results from human cell lines. Thus, further mouse experiments using different UA dosages and treatment times are warranted and may provide valuable insight into the action of UA on the STING signaling pathway.

Together, these results show that UA further enhances the cGAS-STING signaling pathway in response to cytosolic DNA stimulation, possibly through increased STING gene transcription, and that UA may prime the organism for cGAS-STING activation.

3.2. Gene expression analysis identifies the genes and pathways markedly affected by UA

To get a more unbiased analysis on the signaling affected by UA, we used NanoString technology. We employed the human neuroinflammation panel and found that key genes, which control the immune system and inflammatory response were significantly affected by UA (Fig. 2D-J). Meta-analysis in Rosalind (www.rosalind.bio) revealed four clusters, one downregulated (cluster 1, blue) and three upregulated (clusters 2–4, yellow) (Fig. 2D). The average pattern displays the consensus gene expression pattern across the entire dataset (Fig. 2E). Clusters 1 and 2 were responsive to UA (Figs. 2F and 2G) and showed little change in response to DNA. Molecular Signature database terms overrepresented in cluster 1 includes downregulation of the G2/M cell cycle checkpoint (adjusted p-value (p-adj) 7.6e-6) and upregulation of the p53 pathway (p-adj 0.017). Some of the top genes downregulated after UA or UA+DNA treatment include the genes *TOP2A*, *BIRC5*, *DOCK2*, and *LMNB1* from cluster 1 (Fig. 2F). In contrast, *p21* (*CDKN1A*), *MDM2*, *ARC*, *DDB2*, *IL1B*, and *APOE* were among the top upregulated genes changed in response to UA or UA+DNA in cluster 2 (Fig. 2G).

Clusters 3 and 4 constitute upregulated genes changed in both UA and DNA comparisons, which are additive in the UA+DNA comparison. Many microglial genes (33) were also found in clusters 3 and 4 but are shown separately in Fig. 2J, and all were upregulated in the UA+DNA comparison. NF-κB signaling genes were among the top changed genes in cluster 3 including: *RIPK1*, *BCL10*, and *BCL2L1* (Fig. 2H). Inflammatory signaling terms dominated cluster 4 (interferon-γ signaling (p-adj 4.9e-8), interferon-α (p-adj 7.9e-5), and TNFα signaling (p-value 0.001) (Fig. 2I). TNF-α responsive genes included: *RELB*, *IRF1*, *TFNFSF10*, *TRAF1*, and *ATF3* (Figs. 2I and 2J). Top-changed genes found in cluster 4 and in the microglial term include genes in the cytosolic DNA-sensing pathway (*CXCL10*, *CCL5*, *CCL4*, and *STING* (*TMEM173*) (Fig. 2J). Other notable microglial genes were: *ATF3, OAS1*, *CSF1*, *CD68, NLRP3*, and *C3* (Fig. 2J). Among these, C3 and CSF1 play important functions in autophagosome-to-lysosome fusion (King et al., 2019) and phagocytosis (Smith et al., 2013), respectively, which are important for autophagic clearance. We also noted that SQSTM1, an autophagy receptor which participates in the re-localization of ubiquitinylated STING1 to autophagosomes (Prabakaran et al., 2018) was also among the top-changed genes in the comparison of DNA to UA+DNA. Among the 770 neuroinflammation-related genes analyzed, the picture emerges that UA modestly downregulates the cell cycle and upregulates p53 genes while more robustly upregulating multiple inflammatory signaling pathways.

3.3. UA elevates cytosolic DNA clearance

Activated STING stimulates autophagy by promoting autophagosome formation (Liu et al., 2019; Hopfner and Hornung, 2020). Changes in the amount of lipidated LC3-I (LC3-II), a key step in autophagosome formation, have been used as an indicator of autophagy flux (Galluzzi et al., 2017). The level of LC3-II was consistently increased to a detectable level by UA treatment, and was even more prominent in combined DNA- and UA-treated cells (Fig. 3A).

Autophagic clearing of cytoplasmic DNA is thought to be the primordial function of cGAS-STING in the defense against invading microorganisms and viruses (Gui et al., 2019). Thus, we tested the effect of UA treatment on cytosolic DNA clearance using TAMRA-labeled DNA substrates and live-cell microscopy. As DNA-tagged fluorescence is captured from the time of coming into focus in the wells (as opposed to quenched signals), the graphs first show accumulation of signal, and then a decline as substrates are degraded. UA treatment decreased DNA-tagged fluorescence at any given time point, resulting in a significantly decreased total substrate scored over time, as assessed by the area under the curve (Fig. 3B and C). Modification of DNA oligonucleotides at either end has long been used to prevent exonucleolytic degradation of DNA substrates through steric hindrance in biochemical experiments (Eckstein, 2014). Substrate I (TAMRA at 5) had the lowest signal intensity compared with Substrates II and III (Supplementary Figure 4A-D) probably because TAMRA impedes the action of the cytoplasmic 3´−5´exonuclease, TREX1, and as such, Substrates II and III are better protected against TREX1 degradation in the cytoplasm. UA significantly decreased fluorescence from TAMRA-tagged DNA of all three substrates over time, representative images are shown in Supplementary Figure 4E.

Collectively, these results demonstrate that UA is a useful cGAS-STING-promoting compound while also increasing autophagic clearance of cytoplasmic DNA.

3.4. UA affects the overall organization of ER and Golgi

The retention of STING in the ER as well as its transport from the ER to Golgi following binding to cGAMP are largely controlled by ER- and Golgi-associated factors (Lepelley et al., 2020). Thus, we speculated that, in addition to its effect on the expression of STING, UA may also affect the cGAS-STING response through overall organization of these compartments. Immunofluorescence microscopy analysis of calreticulin (ER factor) and TGN (Golgi marker) revealed a significant effect of UA on the spread of both TGN and calreticulin signals without detectable changes in the intensity of the signals (Fig. 3 D-H). This effect was not due to an overall enlargement of the cells, as the nuclear size was not affected (Fig. 3I).

Golga3 (golgin-160) is a member of the family of vesicle tethering proteins to transport vesicles at the Golgi apparatus (Lowe, 2019). Like the calreticulin and TGN results, the Golga3 signaling area, but not the intensity, increased by UA treatment (Supplementary Figure 5). The specificity of the Golga3 antibody used for this study was verified by siRNA knockdown (Supplementary Figure 5D).

UA treatment has been reported to affect mitochondrial dynamics and turnover (Fang et al., 2019). The close association of mitochondria with ER (Wenzel et al., 2022), could suggest that the observed effect of UA on ER organization may be partially through mitochondria. The underlying mechanisms for the effects of UA on ER and Golgi organization warrant further investigation.

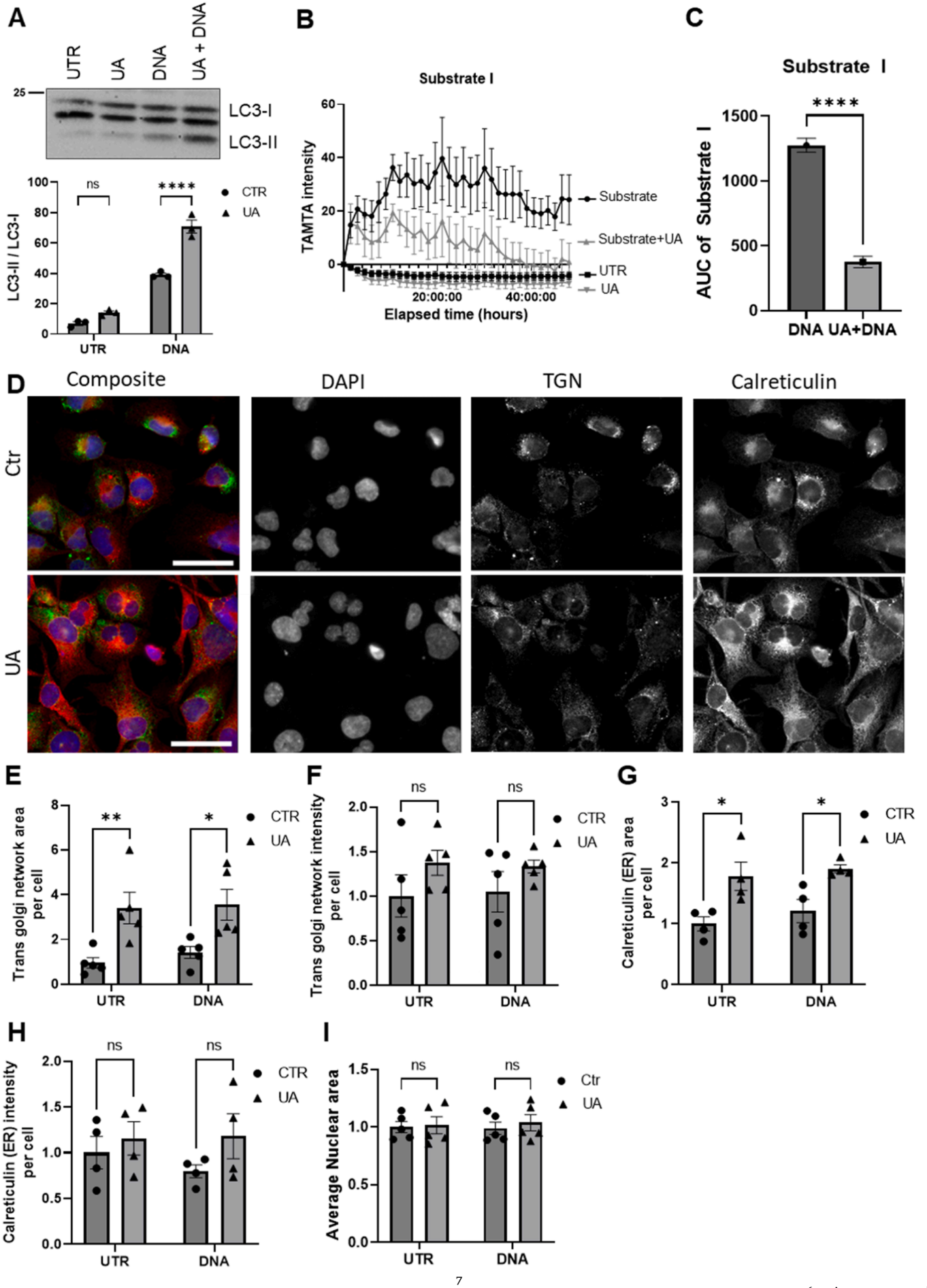

(caption on next page)

Fig. 3. UA stimulates autophagic clearance and affect the organization of the Golgi and endoplasmic reticulum. (A) WB analysis showing elevated level of the autophagosome/autophagy marker LC3-II / LC3-I ratio following UA and/or DNA stimulation of HMC3 cells compared to control (UTR), analyzed by two-way ANOVA (n = 3). (B) HMC3 cells treated with UA scored for TAMRA-tagged DNA degradation over time by live-cell imaging over 48 h, with the area under the curves (AUC) shown in (C) (n = 4). This graph was analyzed by a t-test. (D) Representative images are shown of HMC3 cells stimulated with or without UA (n = 4–5), scalebar = 50 μm. An ImageJ algorithm scored the antibody signals per cell. The area and intensity of the Golgi network (E-F) and the endoplasmic reticulum (G-H) were scored by immunofluorescence using TGN46 and Calreticulin antibodies, respectively. Cell nuclear size was quantified from the same images and shown in (I). Graphs show area or intensity normalized to cell count with two-way ANOVA statistical analysis.

3.5. UA treatment improves the STING signaling pathway in a DNA repair-deficient cancer cell line

Chromosomal instability is a distinct feature of cancer cells, often leading to the release of various forms of nuclear DNA into the cytoplasm (Bakhoum et al., 2018), which could generate an anti-cancer immune response via cGAS-STING signaling (Amouzegar et al., 2021). As several cancers develop strategies to evade cGAS-STING signaling (Xia et al., 2016; Song et al., 2017), the STING-promoting effect of UA in microglial cells, was investigated in a cancer cell line. HCT116 is a DNA mismatch repair-, MLH1-deficient, colon cancer cell line. HCT116 cells show < 100-fold elevated mutation rate and genome instability (Bhattacharyya et al., 1994). As cells contain several DNA sensors on top of cGAS (Zahid et al., 2020), the STING agonist, cGAMP, was used to specifically activate and investigate the cGAS-STING pathway. Treating the HCT116 cells with 30 μM cGAMP for 8 h elevated the level of activated STING but did not lead to significant activation of its downstream binding partners, TBK1 or IRF3 (Fig. 4), suggesting a faulty and impaired STING-mediated IFNI response in these cells. UA treatment significantly increased the level of STING (Fig. 4F) concomitant with elevated pIRF3 and pTBK1 levels in response to UA and cGAMP treatment (Fig. 4).

Taken together, these results demonstrate that UA can potentiate cGAS-STING signaling using a model system where this pathway was clearly defective.

4. Discussion

cGAS-STING innate immune system is a central signaling pathway in the defense against microbial invaders as well as preventing cellular damage to maintain tissue homeostasis. As such, cGAS-STING has attracted much attention as a target of various clinical interventions (Demaria et al., 2019; Amouzegar et al., 2021; Li et al., 2021b). Here we show that UA, an ellagic acid metabolite, is a potent modulator of the cGAS-STING pathway, presenting a natural, non-toxic, compound of relevance in clinical settings.

Following the stimulation and transport toward the trans-Golgi network, STING is eventually degraded (Zhong et al., 2009; Wang

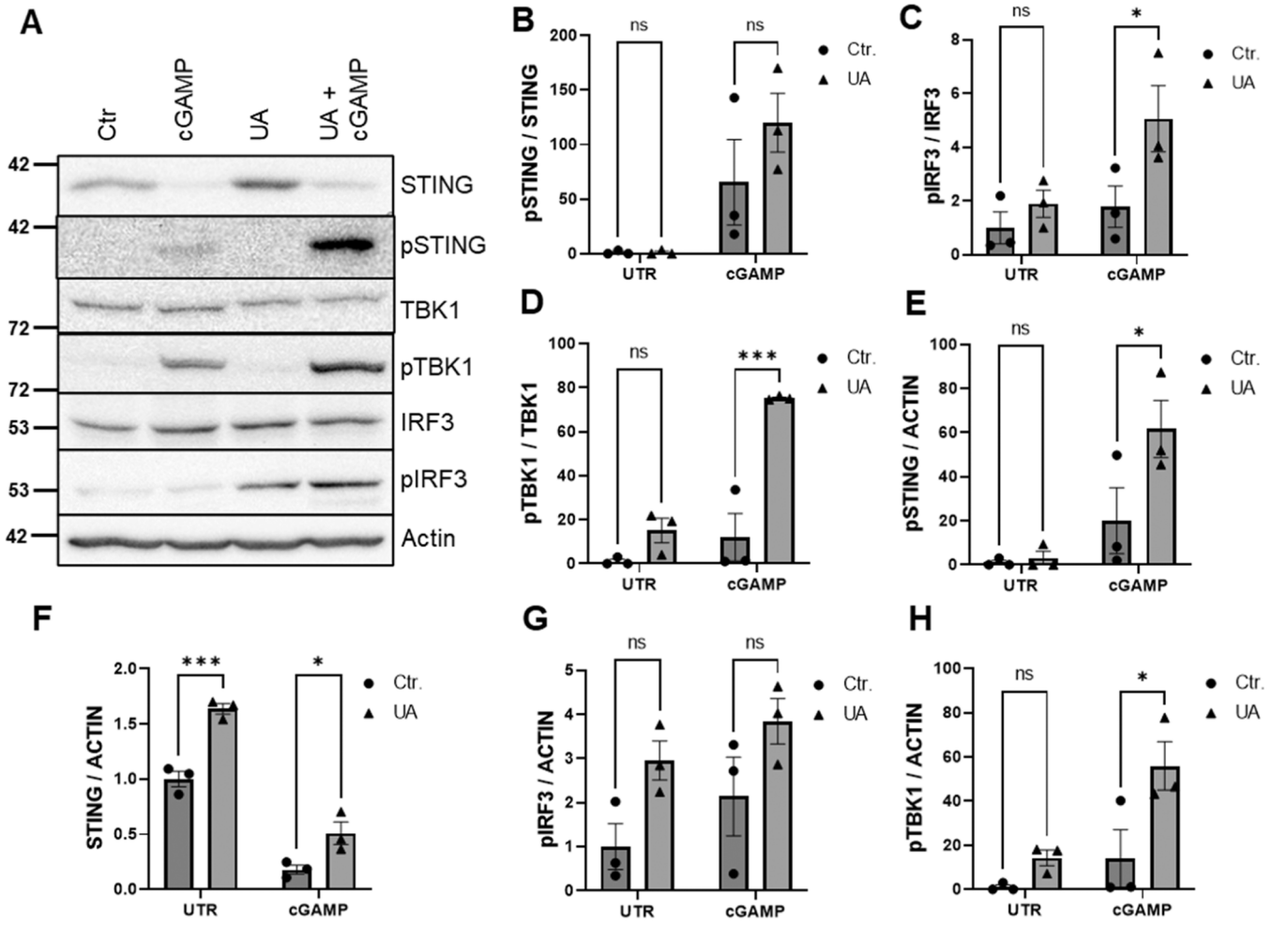

Fig. 4. UA stimulates STING signaling in DNA repair deficient HCT116 colon cancer cells. WB of the colon cancer cell line HCT116 treated with cGAMP alone or in combination with UA for 8 h (A), blotted and quantified for STING (B, E, F), TBK1 (D, H) and IRF3 (C, G) (n = 3). Graphs were analyzed using two-way ANOVA.

et al., 2015). Failure to remove activated STING causes chronic IFNI production and autoimmune disease in humans. This poses a challenge to design agonists that allow controlled spatiotemporal activation of STING. UA treatment increased basal STING mRNA (*TMEM173*) and protein levels without increasing downstream STING signaling, i.e., IRF3 and STAT1 activation by phosphorylation. At the same time, UA treatment enhanced STING signaling in immune-stimulated cells elicited by DNA transfection or cGAMP, by maintaining STING levels (Figs. 1, 2, and 4). Thus, UA treatment would increase the level of available STING that could in turn allow temporary and controlled STING activation.

By western blotting UA alone did not affect the phosphorylation of STING, whereas immunofluorescence imaging picked up a significant stimulation of STING. This could be explained by the higher sensitivity of single cell data by immunofluorescence versus whole cell extracts for immunoblotting. Importantly, no downstream activation of IRF3 was scored in any of the assays by UA treatment alone.

The observed significant stimulation of STING signaling by UA was somewhat unexpected because UA has been reported to possess some anti-inflammatory properties (Toney et al., 2021). Both NanoString and WB analyses showed a positive effect of UA treatment on STING expression (Figs. 1 and 2). The transcription factor NF-κB regulates innate and adaptive immunity and is a central mediator of inflammatory responses (Liu et al., 2017). Our NanoString data showed an overall induction of inflammatory markers by UA treatment, including NF-κB targets (Fig. 2). However, the basal and DNA-stimulated levels of phosphorylation activated NF-κB were consistently reduced by UA treatment in HMC3 cells (Fig. 1A and F-G), in line with some recent reports (Komatsu et al., 2018; Abdelazeem et al., 2021). This apparent partial disconnection between the transcriptional gene expression and protein translation is highly relevant, particularly in inflammatory response investigations that often rely on RNA analysis, and merits further studies.

In addition to promoting the production of IFNI and ISGs, stimulated STING also promotes preautophagosomal membrane formation and autophagy (Gui et al., 2019). Autophagy is the process in which damaged cellular components are isolated in vesicles, which subsequently fuse with lysosomes for enzymatic degradation of their cargo (Galluzzi et al., 2017). Our results support previous reports showing autophagy induction by UA (Zhao et al., 2018), and in addition establish that UA treatment coupled with STING activation is a strong autophagy inducing system, that results in faster clearance of cytosolic DNA (Fig. 3A-C). As the curves for DNA-tagged fluorescence peak at a lower intensity for UA-treated cells compared to control cells, UA-treatment may result in faster initiation of degradation, or this could be a result of a higher level of extracellular proteases. The rate of degradation from the peak was not significantly changed by UA treatment.

cGAS-STING signaling in cancer cells has been an increasingly recognized important mechanism connecting genome instability to immune cell infiltration and inflammation in neoplastic malignant tumors (Woo et al., 2014). Thus, the ability of UA to modulate STING expression and STING's increasingly recognized role in antitumor immune response, makes it a target for immunotherapy (Amouzegar et al., 2021). The colon cancer cell line, HCT116, with DNA mismatch repair deficiency, showed impaired activation of the cGAS-STING pathway (Fig. 4). UA treatment increased the STING level and corrected the STING-dependent activation of IRF3 and TBK1 via cGAMP stimulation (Fig. 4). Given the complex role of the cGAS-STING pathway in different stages of cancer progression (Bakhoum et al., 2018; Hong et al., 2022), it is necessary to further investigate the effects of UA treatment on cancer progression in appropriate mouse models of human cancer with chromosomal instability (Bakhoum et al., 2018; Li et al., 2021a). Of note, it has recently been shown that UA treatment can promote T memory stem cell expansion to promote effective anti-tumor responses in mice (Denk et al., 2022). This effect was shown to rely on UA-mediated induction of autophagic removal of mitochondria called mitophagy. Interestingly, the induction of mitophagy by UA has been shown to result in diverse effects such as prolonged lifespan in C. elegans (Ryu et al., 2016) and improved Tau and Amyloid-β pathology in various models of human Alzheimer's Disease (Fang et al., 2019). However, under our experimental conditions, we did not see any detectable effect of UA-treatment on mitophagy activation (data not shown). Therefore, our data suggests that the effect of UA on restoration of the cGAS-STING signaling pathway in the cancer cell line, is mediated by the increased level of STING.

The aging process is associated with a gradual loss of muscle mass and strength, leading to reduced physical performance and endurance ability. Long-term UA supplementation has proven safe and well tolerated and improved muscle endurance and performance (Liu et al., 2022). Evidence suggests that innate antiviral immunity and IFNI response decline with aging (Bartleson et al., 2021). It will be interesting to investigate whether UA supplementation also improves age-associated decline in antiviral immune response via STING expression and activity, while inhibiting NF-κB activation.

In conclusion, UA treatment stimulates STING transcription and translation, which in turn boosts the IRF3 arm of the cGAS-STING pathway (Fig. 5). In line with STING's primordial function in cytosolic DNA clearance via autophagy (Gui et al., 2019), UA treatment also increased autophagic flux and cytosolic DNA clearance (Figs. 3 and 5). Thus, the use of UA alone or in combination with other pharmacological compounds may present a potential therapeutic approach in the treatment of human diseases that involve aberrant cGAS-STING activation or accumulation of cytosolic DNA and warrants further investigation in relevant transgenic animal models.

Funding and acknowledgements

This work was partly supported by the Intramural Program of the National Institute on Aging, National Institutes of Health, and supported by the Center for Healthy Aging, ICMM, University of Copenhagen and by a grant No 1150171001 from the Novo Nordisk Foundation. We thank Drs. Tomasz Kulikowicz and Mansoor Hussain for critically reading the manuscript.

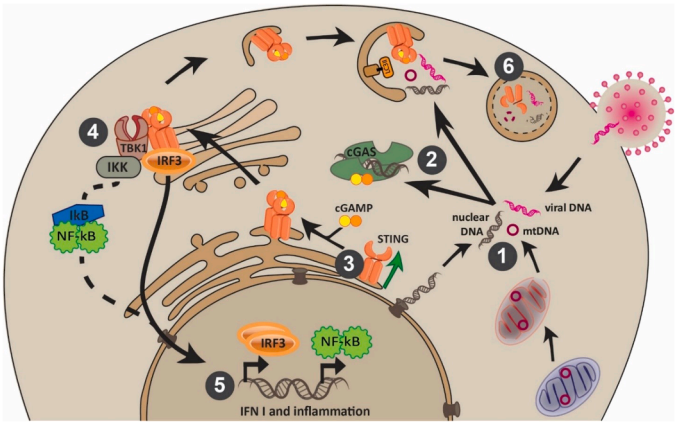

Fig. 5. Mechanistic model of the effect of UA. The cGAS-STING pathway plays a central role in innate and adaptive immune defense and is stimulated via a wide variety of cytosolic DNA (1). TREX1 and the indiscriminate degradation of DNA by autophagy modulate the activation of this pathway, but when enough cytosolic DNA is present, it will trigger cGAS to produce cGAMP (2). cGAMP binds to and activates STING, which is upregulated by UA treatment (3, green arrow). STING then translocates from the ER to the Golgi to bind TBK1. TBK1 phosphorylation can activate IRF3 and NF-κB (via IKK), which both translocate to the nucleus to induce the transcription of IFNI and proinflammatory genes (4 and 5). Following UA pretreatment, the IRF3 arm is favored over NF-κB. To modulate STING activation and cytosolic DNA, STING itself promotes autophagosome biogenesis and subsequent recruitment of lipidated LC3 (LC3II), before being degraded via autophagy (6). UA-stimulated STING expression likewise increases autophagic flux and cytosolic DNA clearance.

Declaration of Competing Interest

The authors declare no conflicts of interest.

Data Availability

Data will be made available on request.

Appendix A. Supporting information

Supplementary data associated with this article can be found in the online version at doi:10.1016/j.mad.2023.111897.

References

Abdelazeem, K.N.M.M., Kalo, M.Z., Beer-Hammer, S., Lang, F., 2021. The gut microbiota metabolite urolithin A inhibits NF-κB activation in LPS stimulated BMDMs. Sci. Rep. 11, 7117 https://doi.org/10.1038/s41598-021-86514-6.

Amouzegar, A., Chelvanambi, M., Filderman, J., Storkus, W., Luke, J., 2021. STING agonists as cancer therapeutics. Cancers 13, 2695. https://doi.org/10.3390/cancers13112695.

Bakhoum, S.F., Ngo, B., Laughney, A.M., Cavallo, J.-A., Murphy, C.J., Ly, P., et al., 2018. Chromosomal instability drives metastasis through a cytosolic DNA response. Nature 553, 467–472. https://doi.org/10.1038/nature25432.

Bartleson, J.M., Radenkovic, D., Covarrubias, A.J., Furman, D., Winer, D.A., Verdin, E., 2021. SARS-CoV-2, COVID-19 and the aging immune system. Nat. Aging 1, 769–782. https://doi.org/10.1038/s43587-021-00114-7.

Bhattacharyya, N.P., Skandalis, A., Ganesh, A., Groden, J., Meuth, M., 1994. Mutator phenotypes in human colorectal carcinoma cell lines. Proc. Natl. Acad. Sci. 91, 6319–6323. https://doi.org/10.1073/pnas.91.14.6319.

Burke, S.J., Goff, M.R., Lu, D., Proud, D., Karlstad, M.D., Collier, J.J., 2013. Synergistic expression of the CXCL10 gene in response to IL-1β and IFN-γ involves NF-κB, phosphorylation of STAT1 at Tyr701, and acetylation of histones H3 and H4. J. Immunol. 191, 323–336. https://doi.org/10.4049/jimmunol.1300344.

Cerdá, B., Periago, P., Espín, J.C., Tomás-Barberán, F.A., 2005. Identification of Urolithin A as a metabolite produced by human colon microflora from ellagic acid and related compounds. J. Agric. Food Chem. 53, 5571–5576. https://doi.org/10.1021/jf050384i.

Demaria, O., Cornen, S., Daëron, M., Morel, Y., Medzhitov, R., Vivier, E., 2019. Harnessing innate immunity in cancer therapy. Nature 574, 45–56. https://doi.org/10.1038/s41586-019-1593-5.

Denk, D., Petrocelli, V., Conche, C., Drachsler, M., Ziegler, P.K., Braun, A., et al., 2022. Expansion of T memory stem cells with superior anti-tumor immunity by Urolithin A-induced mitophagy. Immunity 55 (11), 2059–2073. https://doi.org/10.1016/J.IMMUNI.2022.09.014.

Eckstein, F., 2014. Phosphorothioates, essential components of therapeutic oligonucleotides. Nucleic Acid. Ther. 24, 374–387. https://doi.org/10.1089/nat.2014.0506.

Fang, E.F., Hou, Y., Palikaras, K., Adriaanse, B.A., Kerr, J.S., Yang, B., et al., 2019. Mitophagy inhibits amyloid-β and tau pathology and reverses cognitive deficits in models of Alzheimer's disease. Nat. Neurosci. 22, 401–412. https://doi.org/10.1038/s41593-018-0332-9.

Galluzzi, L., Baehrecke, E.H., Ballabio, A., Boya, P., Bravo-San Pedro, J.M., Cecconi, F., et al., 2017. Molecular definitions of autophagy and related processes. EMBO J. 36, 1811–1836. https://doi.org/10.15252/embj.201796697.

Gao, P., Ascano, M., Wu, Y., Barchet, W., Gaffney, B.L., Zillinger, T., et al., 2013. Cyclic [G(2′,5′)pA(3′,5′)p] is the metazoan second messenger produced by DNA-activated cyclic GMP-AMP Synthase. Cell 153, 1094–1107. https://doi.org/10.1016/j.cell.2013.04.046.

Gui, X., Yang, H., Li, T., Tan, X., Shi, P., Li, M., et al., 2019. Autophagy induction via STING trafficking is a primordial function of the cGAS pathway. Nature 567, 262–266. https://doi.org/10.1038/s41586-019-1006-9.

Hatch, E.M., Fischer, A.H., Deerinck, T.J., Hetzer, M.W., 2013. Catastrophic nuclear envelope collapse in cancer cell micronuclei. Cell 154, 47–60. https://doi.org/10.1016/j.cell.2013.06.007.

Hong, C., Schubert, M., Tijhuis, A.E., Requesens, M., Roorda, M., van den Brink, A., et al., 2022. cGAS–STING drives the IL-6-dependent survival of chromosomally instable cancers. Nature 607, 366–373. https://doi.org/10.1038/s41586-022-04847-2.

Hopfner, K.-P., Hornung, V., 2020. Molecular mechanisms and cellular functions of cGAS–STING signalling. Nat. Rev. Mol. Cell Biol. 21, 501–521. https://doi.org/10.1038/s41580-020-0244-x.

Ishikawa, H., Barber, G.N., 2008. STING is an endoplasmic reticulum adaptor that facilitates innate immune signalling. Nature 455, 674–678. https://doi.org/10.1038/nature07317.

King, B.C., Kulak, K., Krus, U., Rosberg, R., Golec, E., Wozniak, K., et al., 2019. Complement Component C3 is highly expressed in human pancreatic islets and prevents β cell death via ATG16L1 interaction and autophagy regulation. Cell Metab. 29, 202–210.e6. https://doi.org/10.1016/j.cmet.2018.09.009.

Komatsu, W., Kishi, H., Yagasaki, K., Ohhira, S., 2018. Urolithin A attenuates pro-inflammatory mediator production by suppressing PI3-K/Akt/NF-κB and JNK/AP-1 signaling pathways in lipopolysaccharide-stimulated RAW264 macrophages: possible involvement of NADPH oxidase-derived reactive oxygen species. Eur. J. Pharm. 833, 411–424. https://doi.org/10.1016/j.ejphar.2018.06.023.

Konno, H., Konno, K., Barber, G.N., 2013. Cyclic dinucleotides trigger ULK1 (ATG1) phosphorylation of STING to prevent sustained innate immune signaling. Cell 155, 688–698. https://doi.org/10.1016/j.cell.2013.09.049.

Laurent, C., Buée, L., Blum, D., 2018. Tau and neuroinflammation: what impact for Alzheimer's disease and tauopathies? Biomed. J. 41, 21–33. https://doi.org/10.1016/j.bj.2018.01.003.

Lepelley, A., Martin-Niclós, M.J., Le Bihan, M., Marsh, J.A., Uggenti, C., Rice, G.I., et al., 2020. Mutations in COPA lead to abnormal trafficking of STING to the Golgi and interferon signaling. J. Exp. Med. 217 https://doi.org/10.1084/jem.20200600.

Li, J., Duran, M.A., Dhanota, N., Chatila, W.K., Bettigole, S.E., Kwon, J., et al., 2021a. Metastasis and immune evasion from extracellular cGAMP hydrolysis. Cancer Discov. 11, 1212–1227. https://doi.org/10.1158/2159-8290.CD-20-0387.

Li, S., Luo, M., Wang, Z., Feng, Q., Wilhelm, J., Wang, X., et al., 2021b. Prolonged activation of innate immune pathways by a polyvalent STING agonist. Nat. Biomed. Eng. 5, 455–466. https://doi.org/10.1038/s41551-020-00675-9.

Liu, D., Wu, H., Wang, C., Li, Y., Tian, H., Siraj, S., et al., 2019. STING directly activates autophagy to tune the innate immune response. Cell Death Differ. 26, 1735–1749. https://doi.org/10.1038/s41418-018-0251-z.

Liu, K., Lan, Y., Li, X., Li, M., Cui, L., Luo, H., et al., 2020. Development of small molecule inhibitors/agonists targeting STING for disease. Biomed. Pharmacother. 132, 110945 https://doi.org/10.1016/j.biopha.2020.110945.

Liu, S., D'Amico, D., Shankland, E., Bhayana, S., Garcia, J.M., Aebischer, P., et al., 2022. Effect of Urolithin a supplementation on muscle endurance and mitochondrial health in older adults. JAMA Netw. Open 5, e2144279. https://doi.org/10.1001/jamanetworkopen.2021.44279.

Liu, T., Zhang, L., Joo, D., Sun, S.-C., 2017. NF-κB signaling in inflammation. Signal Transduct. Target Ther. 2, 17023 https://doi.org/10.1038/sigtrans.2017.23.

Lowe, M., 2019. The physiological functions of the golgin vesicle tethering proteins. Front Cell Dev. Biol. 7 https://doi.org/10.3389/fcell.2019.00094.

Norden, E., Heiss, E.H., 2019. Urolithin A gains in antiproliferative capacity by reducing the glycolytic potential via the p53/TIGAR axis in colon cancer cells. Carcinogenesis 40, 93–101. https://doi.org/10.1093/carcin/bgy158.

Prabakaran, T., Bodda, C., Krapp, C., Zhang, B., Christensen, M.H., Sun, C., et al., 2018. Attenuation of cGAS-STING signaling is mediated by a p62/SQSTM1–dependent autophagy pathway activated by TBK1. EMBO J. 37. https://doi.org/10.15252/embj.201797858.

Qiu, J., Chen, Y., Zhuo, J., Zhang, L., Liu, J., Wang, B., et al., 2022. Urolithin A promotes mitophagy and suppresses NLRP3 inflammasome activation in lipopolysaccharide-induced BV2 microglial cells and MPTP-induced Parkinson's disease model. Neuropharmacology 207. https://doi.org/10.1016/J.NEUROPHARM.2022.108963.

Ryu, D., Mouchiroud, L., Andreux, P.A., Katsyuba, E., Moullan, N., Nicolet-Dit-Félix, A. A., et al., 2016. Urolithin A induces mitophagy and prolongs lifespan in C. elegans and increases muscle function in rodents. Nat. Med. 2016 22:8 22, 879–888. https://doi.org/10.1038/nm.4132.

Smith, A.M., Gibbons, H.M., Oldfield, R.L., Bergin, P.M., Mee, E.W., Curtis, M.A., et al., 2013. M-CSF increases proliferation and phagocytosis while modulating receptor and transcription factor expression in adult human microglia. J. Neuroinflamm. 10, 859 https://doi.org/10.1186/1742-2094-10-85.

Song, S., Peng, P., Tang, Z., Zhao, J., Wu, W., Li, H., et al., 2017. Decreased expression of STING predicts poor prognosis in patients with gastric cancer. Sci. Rep. 7, 39858 https://doi.org/10.1038/srep39858.

Sun, L., Wu, J., Du, F., Chen, X., Chen, Z.J., 2013. Cyclic GMP-AMP synthase is a cytosolic DNA sensor that activates the Type I interferon pathway. Science (1979) 339, 786–791. https://doi.org/10.1126/science.1232458.

Sun, W., Li, Y., Chen, L., Chen, H., You, F., Zhou, X., et al., 2009. ERIS, an endoplasmic reticulum IFN stimulator, activates innate immune signaling through dimerization. Proc. Natl. Acad. Sci. 106, 8653–8658. https://doi.org/10.1073/pnas.0900850106.

Toney, A.M., Fox, D., Chaidez, V., Ramer-Tait, A.E., Chung, S., 2021. Immunomodulatory role of urolithin a on metabolic diseases. Biomedicines 9, 192. https://doi.org/10.3390/biomedicines9020192.

Vashi, N., Bakhoum, S.F., 2021. The evolution of STING signaling and its involvement in cancer. Trends Biochem Sci. 46, 446–460. https://doi.org/10.1016/j.tibs.2020.12.010.

Wang, Y., Lian, Q., Yang, B., Yan, S., Zhou, H., He, L., et al., 2015. TRIM30α is a negative-feedback regulator of the intracellular DNA and DNA virus-triggered response by targeting STING. PLoS Pathog. 11, e1005012 https://doi.org/10.1371/journal.ppat.1005012.

Wenzel, E.M., Elfmark, L.A., Stenmark, H., Raiborg, C., 2022. ER as master regulator of membrane trafficking and organelle function. J. Cell Biol. 221 https://doi.org/10.1083/jcb.202205135.

Woo, S.-R., Fuertes, M.B., Corrales, L., Spranger, S., Furdyna, M.J., Leung, M.Y.K., et al., 2014. STING-dependent cytosolic DNA sensing mediates innate immune recognition of immunogenic tumors. Immunity 41, 830–842. https://doi.org/10.1016/j.immuni.2014.10.017.

Wu, J., Sun, L., Chen, X., Du, F., Shi, H., Chen, C., et al., 2013. Cyclic GMP-AMP Is an endogenous second messenger in innate immune signaling by cytosolic DNA. Science (1979) 339, 826–830. https://doi.org/10.1126/science.1229963.

Xia, T., Konno, H., Ahn, J., Barber, G.N., 2016. Deregulation of STING signaling in colorectal carcinoma constrains DNA damage responses and correlates with tumorigenesis. Cell Rep. 14, 282–297. https://doi.org/10.1016/j.celrep.2015.12.029.

Zahid, A., Ismail, H., Li, B., Jin, T., 2020. Molecular and structural basis of DNA sensors in antiviral innate immunity. Front Immunol. 11, 3094. https://doi.org/10.3389/FIMMU.2020.613039/BIBTEX.

Zhao, W., Shi, F., Guo, Z., Zhao, J., Song, X., Yang, H., 2018. Metabolite of ellagitannins, urolithin A induces autophagy and inhibits metastasis in human sw620 colorectal cancer cells. Mol. Carcinog. 57, 193–200. https://doi.org/10.1002/mc.22746.

Zhong, B., Zhang, L., Lei, C., Li, Y., Mao, A.-P., Yang, Y., et al., 2009. The ubiquitin ligase RNF5 regulates antiviral responses by mediating degradation of the adaptor protein MITA. Immunity 30, 397–407. https://doi.org/10.1016/j.immuni.2009.01.008.